Phase Transition Method To Form Group 6A Nanoparticles on Carbonaceous Templates

Hee-Chang Youn,[†,⊥] Jong-Pil Jegal,[†,⊥] Sang-Hoon Park,[†] Hyun-Kyung Kim,[†] Ho Seok Park,[‡] Kwang Chul Roh,[§,*] and Kwang-Bum Kim[†,*]

[†]Department of Materials Science and Engineering, Yonsei University, 134 Shinchon-dong, Seodaemoon-gu, Seoul 120-749, Republic of Korea, [‡]Department of Chemical Engineering, College of Engineering, Kyung Hee University, 1 Seocheon-dong, Giheung-gu, Yongin-si, Gyeonggi-do 446-701, Republic of Korea, and [§]Energy Efficient Materials Team, Energy & Environmental Division, Korea Institute of Ceramic Engineering & Technology, 233-5 Gasan-dong, Guemcheon-gu, Seoul 153-801, Republic of Korea. [⊥]These authors contributed equally.

ABSTRACT Considerable effort has been made to develop unique methods of preparing and characterizing nanoparticles and nanocomposites in order to exploit the true potential of nanotechnology. We used a facile, versatile phase-transition method for forming Group 6A nanoparticles on carbonaceous templates to produce homogeneous 5–10 nm diameter Group 6A nanoparticles on carbon nanotubes (CNTs) and reduced graphene oxide (RGO), to obtain nanocomposites. The method involved melting and recrystallizing mixtures of elemental sulfur and either CNTs or RGO on carbonaceous templates. The surface tension and hydrophilicity of the molten Group 6A species surfaces and the oxygen functional groups on the carbonaceous template surfaces were considered in depth to provide important guidelines for forming Group 6A nanoparticles on carbonaceous templates. The surface tension of the molten Group 6A species should be intrinsically low, leading to effective wetting on the carbonaceous template. In addition, the molten Group 6A species hydrophilic surfaces were essential for enabling hydrophilic–hydrophilic interaction for selective wetting at the oxygen functional groups on the carbonaceous template, leading to the heterogeneous nucleation of nanoparticles. Furthermore, the size and morphology (isolated *vs* layer-like) of the Group 6A nanoparticles were tuned by adjusting the oxidation state of the carbonaceous template. We investigated the potential application of the nanocomposites prepared using this method to cathode materials in lithium–sulfur secondary batteries.

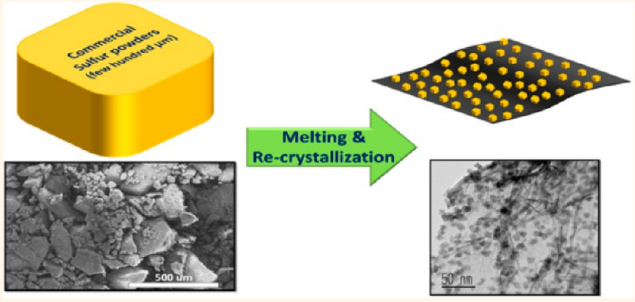

KEYWORDS: Group 6A nanoparticles · carbonaceous template · phase transition method · melting · recrystallization · lithium secondary battery

Numerous scientists and engineers researching nanotechnology have recently endeavored to develop carbon-based nanocomposites showing unique chemical, mechanical, and physical properties,[1] which can lead to nanocomposites showing versatile, tunable material properties and performances far beyond those of their individual counterpart materials. Thus, using nanostructured carbonaceous components to develop nanocomposites will enhance the electron transport rate and provide superior electrolyte contact areas for applications such as catalysts, chemical sensors, and electrochemical devices including lithium secondary batteries and supercapacitors.[2,3]

Scalable, facile solution-based wet-chemical and solid-state methods of synthesizing carbon-based nanocomposites have been developed to exploit the advantages of carbon-based nanocomposites for various potential applications. Solution-based wet-chemical methods such as sol–gel, solvothermal, and co-precipitation syntheses have conventionally been generally used[4–7] since they enable nanocomposites to uniformly and heterogeneously nucleate and grow on carbonaceous templates. Consequently, there have been few reports to date on the use of solid-state methods since it is difficult to use them in order to grow uniform tunable-sized nanoparticles on carbonaceous templates. Hence, using solid-state methods to produce nanocomposites is very challenging.

Group 6A elements such as sulfur and selenium have attracted considerable attention

* Address correspondence to kbkim@yonsei.ac.kr, rkc@kicet.re.kr.

Received for review October 29, 2013 and accepted February 5, 2014.

Published online February 05, 2014
10.1021/nn405633p

© 2014 American Chemical Society

in various fields, so they are attractive candidates for producing nanocomposites. For example, sulfur is important in producing pharmaceuticals, gas sensors, catalysts, and lithium secondary batteries,[8−11] and selenium is important in producing electronic and photonic devices, catalysts, sensors, biotechnology applications, and lithium secondary-batteries.[12−15] In addition, numerous efforts have been made to produce Group 6A nanoparticles and their nanocomposites on carbonaceous substrates in order to produce various high-performance applications. Two methods of synthesizing Group 6A nanocomposites on carbonaceous substrates are widely used. Bottom-up synthesis involves using a solution-based wet-chemical method and a Group 6A containing precursor such as $Na_2S_2O_3$ or Na_2S for sulfur[16−18] or H_2SeO_3 for selenium.[15,19] Top-down synthesis involves using a solid-state method and as-prepared Group 6A nanoparticles and carbonaceous substrates.[20−22] Group 6A nanocomposites previously produced using solution-based wet-chemical methods have required multiple steps, time-consuming processes, and hazardous reaction media such as strong acids. Furthermore, these methods have not yet yielded <50 nm Group 6A nanoparticles on carbonaceous templates.[16,18] Similarly, the solid-state methods of producing Group 6A nanocomposites on carbonaceous materials have only been used to form layer-like morphologies, not Group 6A nanoparticles on carbonaceous templates.[21,23] Therefore, neither synthesis method has yielded <50 nm Group 6A nanoparticles on carbonaceous materials to date possibly because there has not been any in-depth consideration of the surface chemistry of molten carbonaceous materials and Group 6A species.

We developed a facile, versatile phase-transition method of anchoring Group 6A nanoparticles onto carbonaceous materials (carbon nanotubes [CNTs] and reduced graphene oxide [RGO]). The method involves the solid−liquid−solid transition of Group 6A species such as sulfur and selenium on carbonaceous templates. Molten sulfur and selenium are highly appropriate for the solid-state method of producing nanocomposites on carbonaceous materials owing to their low melting points, low surface tensions, and hydrophilic surfaces. Furthermore, Haitao Lui *et al.* recently published a paper in which they claimed that graphene surfaces were in fact hydrophilic.[24] They appeared to be hydrophobic only because of airborne contaminants (hydrocarbons) that adsorb onto the surface. Further, they investigated the effects of heating the graphene to remove the airborne contaminants, thereby producing a hydrophilic graphene surface. According to their results, heating the graphene used in this study should help produce hydrophilic carbonaceous template surfaces by eliminating airborne contaminants (hydrocarbons), enhancing the wettability of the molten Group 6A species on the carbonaceous materials.

It is necessary to clearly understand the interactions at the interface between the molten Group 6A species and the oxygen functional groups on carbonaceous template surfaces in order to use this method to assemble Group 6A nanoparticles on carbonaceous templates. The hydrophilic oxygen functional groups on the carbonaceous template surface could enable the molten Group 6A species to selectively wet through hydrophilic−hydrophilic interactions, generating a number of pinning points for heterogeneously nucleating nanoparticles on the template. Interestingly, the particle sizes and morphologies (*i.e.*, isolated *vs* layer-like) of the resulting nanocomposite were significantly governed by the carbonaceous template oxidation state. Further, we demonstrated that the obtained materials could be used as cathode active materials in lithium−sulfur secondary batteries and that the nanocomposites prepared using our method could be used in other applications such as gas sensors, catalysts, and so on.

RESULTS AND DISCUSSION

Scheme 1 illustrates the proposed synthesis route for anchoring sulfur nanoparticles onto carbonaceous templates. It is a solid-state method involving the phase-transition of Group 6A species at the oxygen functional groups on the carbonaceous templates. We initially prepared the RGO as an underlying template by irradiating graphite oxide with microwaves to produce homogeneous sulfur nanoparticles on the RGO template.[25] The as-prepared RGO template was a suitable substrate on which to anchor the sulfur nanoparticles because its moderate number of oxygen functional groups enabled the molten sulfur to selectively wet at isolated pinning points to form nucleation sites.[26,27] Furthermore, the as-prepared RGO template provided a large specific surface area (~792 m^2/g) (Figure S3, Supporting Information) and high electric conductivity (704 S/m). The details of the method of preparing the RGO are provided in the Experimental Method section. Commercial sulfur and RGO powders were ball-milled to produce a uniform mixture, which was subsequently heated for 4 h at 160 °C, above the melting point of elemental sulfur (119 °C). The molten sulfur selectively located at the hydrophilic sites on the RGO sheets showing oxygen functional groups[26] because it showed low surface tension (<61 mN/m) and a hydrophilic surface caused by the ring-opening-induced transformation of the cycloocta structure into the chain one.[28,29] The mixture was rapidly cooled to nucleate and recrystallize the molten sulfur on the RGO sheets.

Figure 1a shows a scanning electron microscopy (SEM) image and the corresponding energy dispersive X-ray (EDX) elemental mapping of the sulfur nanoparticle/RGO composites prepared by melting and recrystallizing the sulfur/RGO powder mixture on the

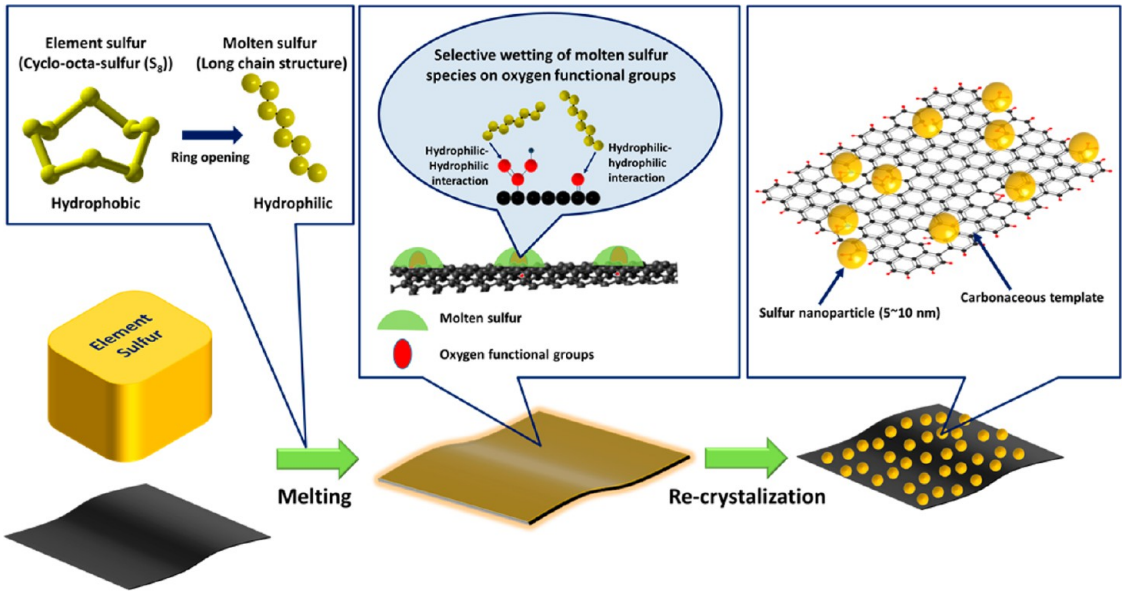

Scheme 1. Schematic illustrating method involving melting and recrystallization to evenly decorate RGO with sulfur nanoparticles.

RGO sheets. The sulfur was uniformly dispersed along the RGO surface in the nanocomposites, which showed highly developed porous structures, as shown in the EDX elemental mapping in the inset of Figure 1a. Furthermore, the morphology of the sulfur nanoparticle/RGO composites was identical to that of the RGO (Figure S1a, Supporting Information), indicating that ball-milling and heating the powder mixtures had not deteriorated the morphology. Transmission electron microscopy (TEM) was used to investigate the microstructure of the sulfur nanoparticle/RGO composite in further detail. Figure 1b,c clearly indicates that the 5−10 nm sulfur nanoparticles were well dispersed and uniformly covered the RGO sheets. The few hundred micrometer in diameter commercial sulfur particles (Figure S2b, Supporting Information) were reduced to 5−10 nm diameter sulfur nanoparticles loaded with approximately 68 wt % sulfur, as indicated by the results of the thermogravimetric analysis (Figure S3, Supporting Information). This synthesis method can be used to easily tune the amount of sulfur loaded onto the RGO sheets by adjusting the ratio of the commercial sulfur and RGO powders in the initial mixture (Figure S4, Supporting Information).

The high-resolution TEM image (Figure 1c) shows a clear lattice fringe, demonstrating the well-crystallized sulfur nanoparticle structures (particles #1 and #2) in the nanocomposites, which is consistent with the X-ray diffraction (XRD) pattern (Figure 1d). The regular 0.286 and 0.344 nm spacings of the lattice planes obtained from the direct line scanning analysis shown in the inset of Figure 1c are consistent with the *d*-spacings of the (044) and (026) planes for sulfur particles #1 and #2, respectively. Figure 1d shows XRD patterns typical of melted and recrystallized sulfur nanoparticle/RGO composites. The intensities and positions of the peaks attributed to the sulfur nanoparticles can be clearly indexed to cyclooctasulfur (S_8), indicating an orthorhombic structure showing the *Fddd* space group (JCPDS #08-0247) and a weak, broad signal around 23°, corresponding to the (002) plane characteristic of RGO. The XRD pattern indicates that the elemental sulfur had not structurally changed and that the RGO had not restacked when the sample was prepared.

Raman spectroscopy was also used to analyze the RGO and sulfur nanoparticles in the composite. The five dominant peaks in the Raman spectra in Figure 1e are as follows: The sulfur nanoparticles exhibit three characteristic peaks at 156, 221, and 473 cm^{-1} Raman shifts, corresponding to an orthorhombic crystal structure consisting of S_8 molecules whose unit cell dimensions are a = 1.045, b = 1.2884, and c = 2.446 nm (powder diffraction card number 8-247, International Center for Diffraction Data, Newton Square, PA, USA).[30] The relative peak intensities of the D band, which represents the structural defects and imperfections, and the G band, which represents the graphitic carbon on the RGO sheets, at 1359 and 1598 cm^{-1}, respectively, are an indication of the degree of graphitization of the carbonaceous materials.[31,32] The ratio of the D to G band intensities (I_D/I_G) was as high as 1.25, similar to that for the as-prepared RGO, indicating that the RGO and molten sulfur had chemically interacted without deteriorating the graphitic domain structure on the RGO sheets.

Furthermore, X-ray photoelectron spectroscopy (XPS) was used to investigate the chemical composition and bonding between the sulfur nanoparticles and the RGO sheets. Figure 1f shows the deconvoluted O 1s peaks obtained from the as-prepared RGO and the sulfur nanoparticle/RGO composite. These spectra

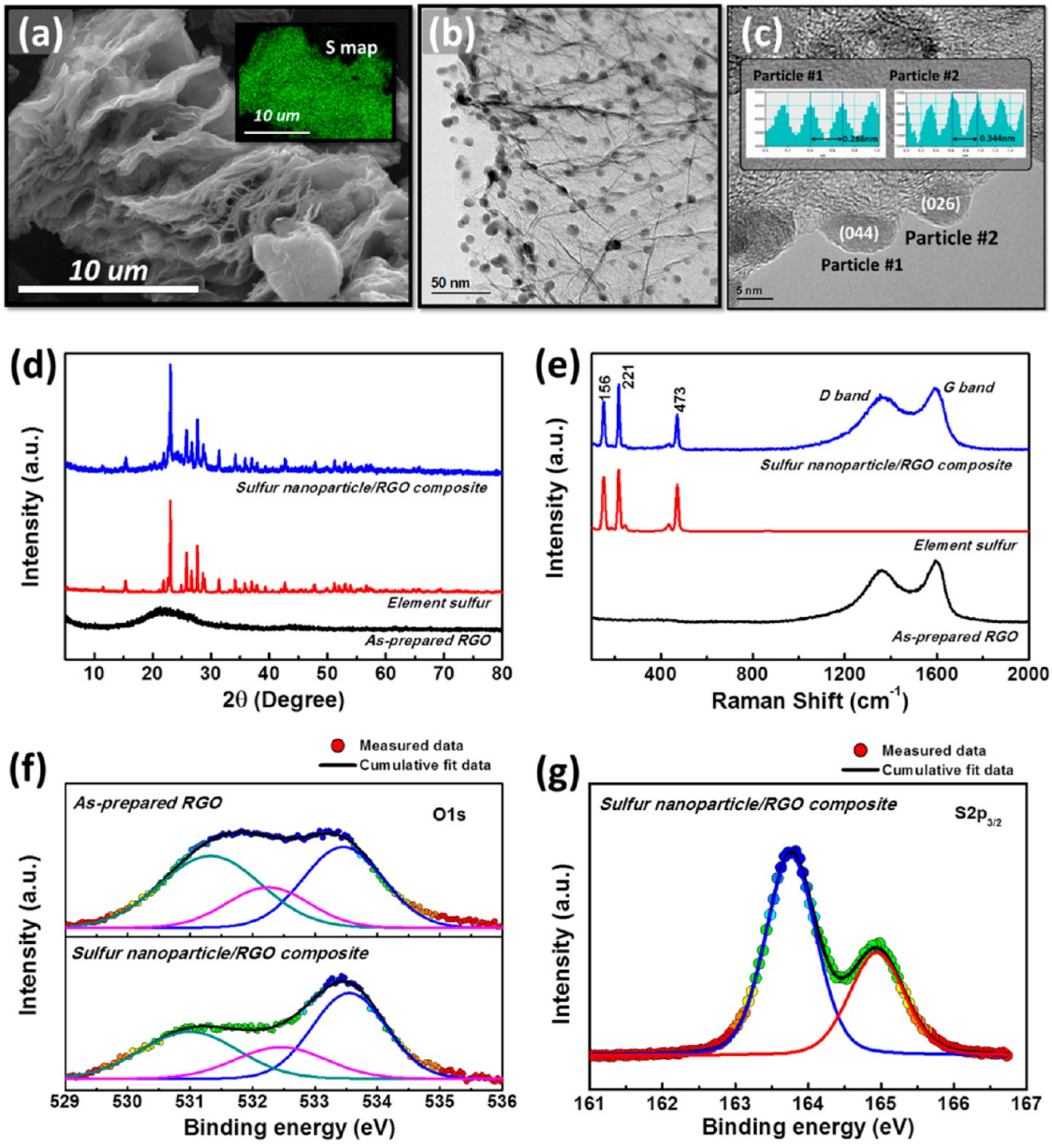

Figure 1. Morphological characterization of sulfur nanoparticle/RGO composite: (a) SEM image (×5000; inset: EDX elemental mapping); (b) TEM and (c) high-resolution TEM images (×500 000). Structural and chemical characterization of sulfur nanoparticle/RGO composite: (d) XRD patterns for as-prepared RGO (black), elemental sulfur (red), and sulfur nanoparticle/RGO composite (blue); (e) Raman spectra for as-prepared RGO (black), elemental sulfur (red), and sulfur nanoparticle/RGO composite (blue); and (f) deconvoluted O 1s XPS profiles acquired from as-prepared RGO (top) and sulfur nanoparticle/RGO composite (bottom) and deconvoluted S $2p_{3/2}$ XPS profile acquired from sulfur nanoparticle/RGO composite.

TABLE 1. Morphological Features of Composite Materials Prepared from Molten Group 6A Species with Different Surface Tensions on Carbonaceous Materials with Different C/O Ratios

carbon type	post treatment	Group 6A	surface tension (mN/m)	carbon content[a] (atom %)	oxygen content[a] (atom %)	C/O ratio	morphological features
CNT (1D)	None	S	61	99.2	0.8	124	Not formed
	Acid treatment	S	61	95.1	4.9	19.4	Nanoparticles (5−10 nm)
RGO (2D)	Heat treatment	S	61	97.3	2.7	36.45	Nanoparticles (5−10 nm)
	None	S	61	90.8	9.2	9.87	Nanoparticles (20−30 nm)
	Acid treatment	S	61	81.8	18.2	4.49	Layers
	None	Se	97	90.8	9.2	9.87	Nanoparticles (<50 nm)
	None	Te	190	90.8	9.2	9.87	Not formed

[a] Carbon and oxygen contents obtained from full-scale XPS spectra of each carbonaceous material.

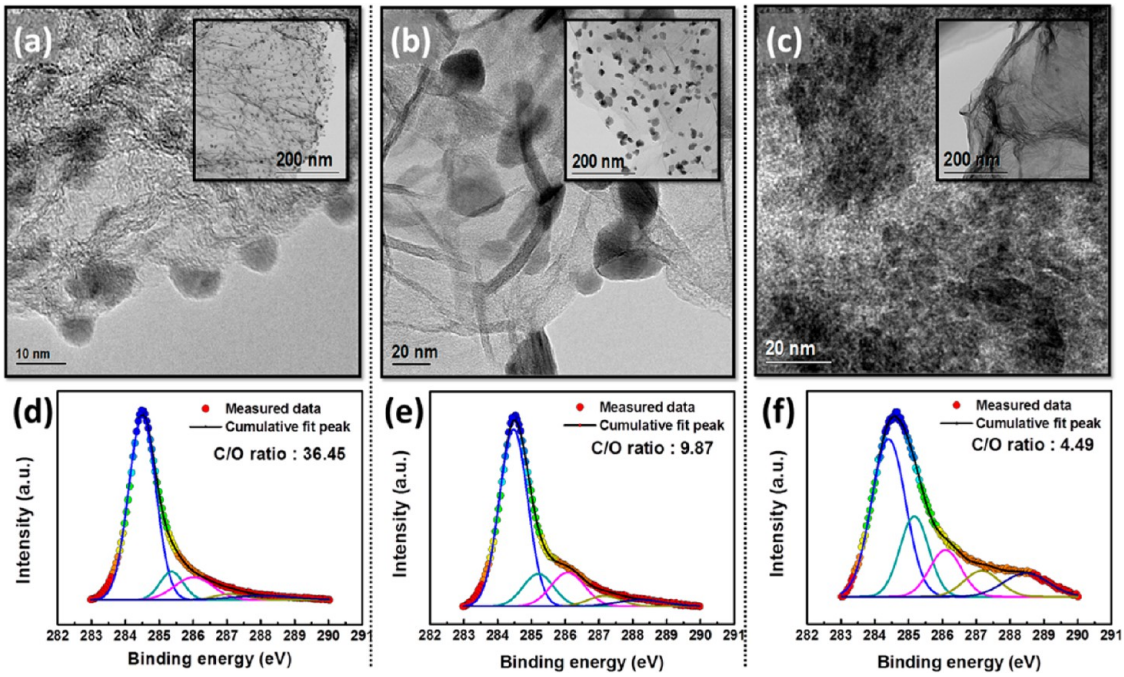

Figure 2. Tuning nanoparticle morphology and size. Isolated nanoparticles *vs* layer-like morphology of elemental sulfur in composites, as determined from the concentration of oxygen functional groups on carbonaceous (RGO sheets) templates. High-resolution TEM images of sulfur/RGO composites (insets: TEM images magnified ×33 000) prepared from RGO templates: (a) sulfur nanoparticle/HRGO900 composite on low-oxidation-state HRGO900 template (C/O ratio, 36.45), (b) sulfur nanoparticle/RGO composite on medium-oxidation-state as-prepared RGO template (C/O ratio, 9.87), and (c) sulfur nanolayer/a-RGO composite on high-oxidation-state a-RGO template (C/O ratio, 4.49). Deconvoluted C 1s XPS profiles for carbonaceous templates indicating various oxidation states: (d) HRGO900 (low), (e) as-prepared RGO (medium), and (f) a-RGO (high).

contain three predominant component peaks at 531.5, 532.5, and 533.3 eV, corresponding to doubly bonded oxygen in carboxyl and ketone groups (O═C−OH or C═O), singly bonded oxygen in carboxyl or ester groups (O═C−OH or O═C−OR), and singly bonded oxygen in hydroxyl or epoxy groups (C−OH or C−O−C), respectively.[33,34] All the oxygen functional groups anchored on the RGO sheets might have contributed to the chemical bonding between the sulfur nanoparticles and the RGO sheets. However, the doubly bonded oxygen in the carboxyl and ketone groups were the main contributors to the chemical bonding because these components showed peak intensities lower than those for RGO in the deconvoluted O 1s XPS spectrum. In addition, the deconvoluted S $2p_{3/2}$ XPS spectrum indicated two peaks at 163.8 and 164.8 eV binding energies, which could be ascribed to C−S or S−S bonds and to S−O chemical bonding, respectively.[17,35] These results strongly indicate that the sulfur was chemically bonded to the RGO sheet and that the formation of sulfur nanoparticles had significantly affected the oxygen functional groups on the RGO sheets.

The concentration of oxygen functional groups on the RGO sheets was modified either by further heating the as-prepared RGO powders at 900 °C in an Ar atmosphere (HRGO900, low-oxidation) or by treating them with nitric acid (a-RGO, high oxidation) to determine how the oxygen functional groups affected sulfur nanoparticle preparation. The differences in the concentrations of oxygen functional groups on the post-treated RGO sheets were demonstrated by investigating the deconvolution of C 1s XPS spectra, as shown in Figure 2d−f. The peak intensity at the higher binding energy, corresponding to the oxygen functional groups on the RGO sheets, in the deconvoluted C 1s XPS spectra decreased when the RGO sheets were heated, indicating that heating had further decreased the concentration of oxygen functional groups anchored on the RGO sheets.

In addition, the C/O ratios of the three RGO samples were calculated from the full-scale XPS spectra for each sample (Figure S5, Supporting Information). The nanocomposites prepared from the HRGO900 and as-prepared RGO samples exhibiting low and medium oxidation (C/O ratio = 36.45 and 9.87 for the low and medium oxidation samples, respectively) showed isolated sulfur nanoparticles evenly dispersed on the RGO sheets (Figure 2a,b). The sulfur nanoparticles attached on the HRGO900 and RGO sheets also showed different sizes, reflecting the different oxidations of the carbonaceous materials. Isolated 5−10 nm sulfur nanoparticles were loaded on the low-oxidation HRGO900 sheets, as indicated by the high-resolution TEM images shown in Figure 2a. Larger (20−30 nm) sulfur nanoparticles were well dispersed on the medium-oxidation RGO sheets. These results suggest that the size of the

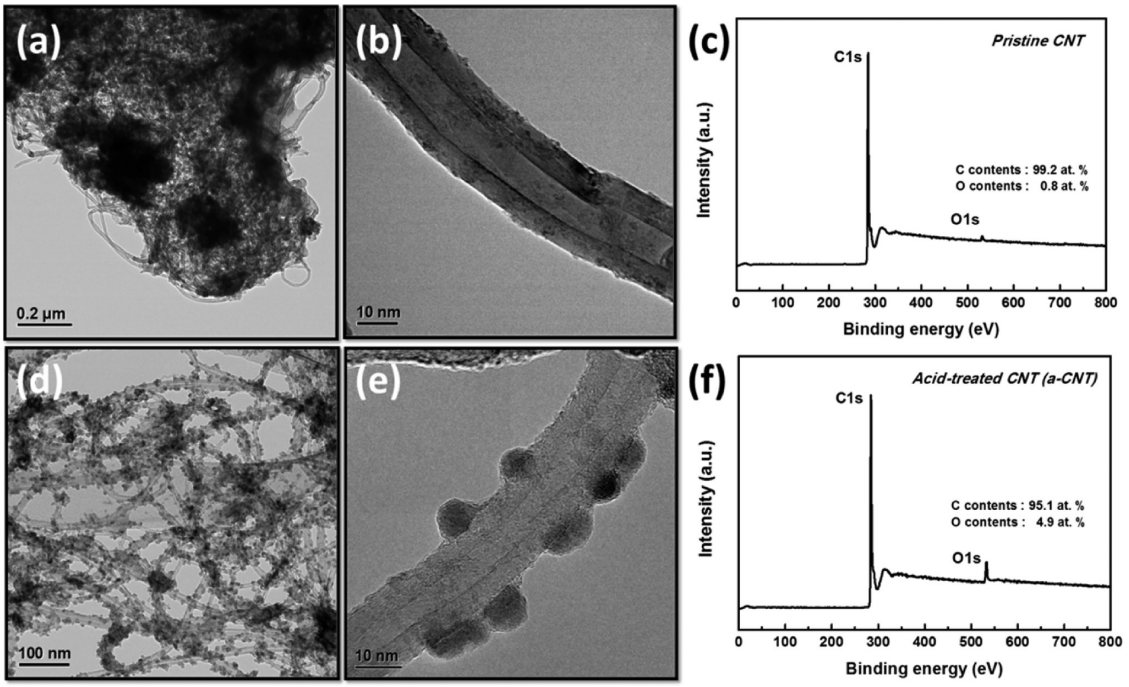

Figure 3. Effects of oxygen functional groups on wetting and formation of sulfur nanoparticles on 1D carbonaceous CNTs. Oxygen functional groups clearly form uniform elemental sulfur nanoparticles on CNT surfaces. (a and b) TEM images of sulfur composites produced using pristine CNTs as template, indicating that no sulfur particles had formed on CNT surfaces. (c) Full-scale XPS profile for pristine CNTs, indicating that CNT surfaces did not show any oxygen functional groups. (d and e) TEM images of sulfur composites prepared using acid-treated CNTs (a-CNTs) as template, indicating that highly uniform sulfur nanoparticles as large as 5−10 nm had formed on a-CNT surfaces. (f) Full-scale XPS profile for a-CNTs, indicating that carbonaceous surface treated with nitric acid showed 4.9 atom % oxygen functional groups.

sulfur particles on the carbonaceous template might strongly depend on the template oxidation state. The composite material prepared from the high-oxidation a-RGO (C/O ratio = 4.49) tended to exhibit a layer-like morphology formed by numerous small interconnected sulfur nanoparticles (Figure 2c) on the a-RGO sheets. Numerous oxygen functional groups on the a-RGO sheets enables numerous nanoparticles to nucleate and agglomerate along the a-RGO surface because the oxygen functional groups act as pinning points and nucleation sites for molten sulfur. The oxygen functional groups on the RGO sheets were strongly associated with the formation of sulfur nanoparticles when the sulfur/RGO powder mixture was melted and recrystallized. Furthermore, the particle size and morphology could be easily tuned by adjusting the concentration of oxygen functional groups on the RGO sheet in order to obtain isolated nanoparticles or layer-like structures consisting of interconnected nanoparticles on the RGO surface. These results indicate that a considerable concentration of oxygen functional groups (<10 wt.%) on the carbonaceous surface provided sites where sulfur nanoparticles could heterogeneously nucleate without agglomerating, so the oxygen groups had acted like the dispersion media used in the wet-chemical method of preparing isolated nanoparticles.

Additional experiments were performed using different carbonaceous materials such as pristine CNTs, acid-treated CNTs (a-CNTs), and chemically reduced graphene oxide (CRGO) as substrates. Comparing the wettabilities of the molten sulfur on the pristine CNTs and a-CNTs clearly demonstrated the effects of the oxygen functional groups on the wettability of the molten sulfur and on the production of sulfur nanoparticles on carbonaceous materials. Figure 3c,d show TEM images of the sulfur/a-CNT composite prepared using the same method used to prepare the sulfur nanoparticle/RGO composites. Several 5−10 nm sulfur nanoparticles were uniformly dispersed along the a-CNT surface (4.9 atom % oxygen; Figure S6). As shown in Figure 3a,b, no sulfur particles had been deposited onto the pristine CNT surface when the identical synthesis method was used since the pristine CNTs (0.8 atom % oxygen; Figure S6) show hydrophobic surfaces, *i.e.*, they do not have any oxygen functional groups, so the sulfur showed negligible wettability and the CNT surface did not show any pinning points where the molten sulfur could nucleate. Sulfur was easily deposited onto the CRGO surface of the sulfur/CRGO composites heated at 160 °C, as demonstrated by SEM, EDX elemental mapping, and EDX spectroscopy (Figure S7, Supporting Information), since the CRGO surface shows a moderate number of oxygen functional groups. The TEM image of the CRGO surface shows a layer-like morphology analogous to that of the sulfur nanoparticle/RGO composite prepared using high-oxidation RGO (C/O ratio = 4.49).

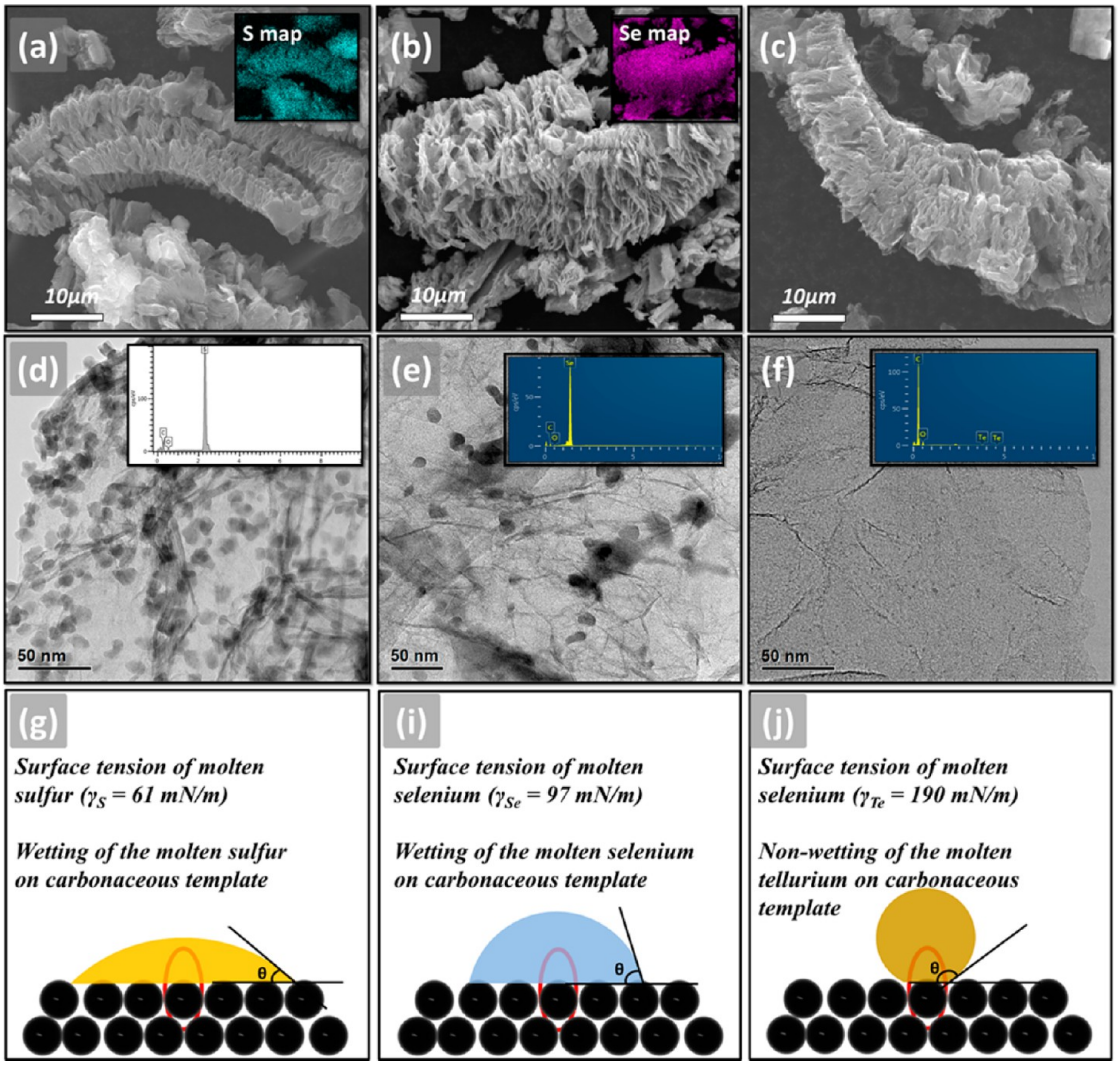

Figure 4. Effect of molten species surface tension on wetting and formation of Group 6A nanoparticles on carbonaceous templates. (a−c) SEM images of Group 6A composites prepared using phase-transition method and (a) sulfur, (b) selenium, and (c) tellurium. (d−f) TEM images of Group 6A composites containing (d) sulfur, (e) selenium, and (f) tellurium. (g−j) Schematics diagraming surface-tension-based wetting of molten Group 6A species on carbonaceous materials: (g) sulfur (γ = 61 mN/m), (i) selenium (γ = 97 mN/m), and (j) tellurium (γ = 190 mN/m).

We extended the same method to molten elemental selenium and tellurium to determine whether the method could be used to produce other nanocomposites consisting of carbonaceous materials and molten Se or Te, which are also Group 6A (chalcogen) elements. Figure 4 shows the morphologies of the Group 6A/RGO nanocomposites (as determined using SEM, EDX mapping, EDX spectroscopy, and high-resolution TEM) and schematics diagraming the surface-tension-based wetting behavior of each molten Group 6A species on the carbonaceous materials. In particular, we clearly demonstrated the effect of the molten Group 6A species surface tension (γ) on the formation of nanocomposites on carbonaceous materials. The wetting of the molten species on 2−20 nm diameter CNTs has already been examined in detail and reported elsewhere in the literature.[29,36] The previous report clearly demonstrated that the upper limit for the molten species surface tension was $\gamma \approx 180$ mN/m, beyond which molten species wetting on CNTs was no longer favorable.[36] The molten S, Se, and Te showed calculated surface tensions of 61, 97, and 190 mN/m, respectively.[29,36] As shown in Figure 4b,e, the Se nanoparticle/RGO composite could be prepared using this method, because Se shows relatively low surface tension (γ = 97 mN/m) and because the molten composite shows a hydrophilic surface, which leads to effective wetting on a carbonaceous surface and selective pinning at the oxygen functional groups to produce the nanocomposite. However, the Te/RGO composite could not be prepared using this method because Te shows high surface tension (γ = 190 mN/m), which leads to negligible wetting on carbonaceous materials, as shown in Figure 4c,f.

The resulting sulfur nanoparticle/RGO composite prepared using this method could potentially be used

as a cathode material in a lithium−sulfur secondary battery. The electrochemical performances of the coin-cell-configured sulfur nanoparticle/RGO composites was evaluated by dissolving 1 M $LiCF_3SO_3$ and 0.2 M $LiNO_3$ in tetra(ethylene glycol) dimethyl ether (TEGDME) and 1,3-dioxolane (DOL) mixed in a 1:1 volumetric ratio. Figure 5a shows the galvanostatic charge/discharge profile for the sulfur nanoparticle/RGO composite, which is typical of a Li/S battery. Two voltage plateaus consistent with the mechanism for the reduction and oxidation of sulfur during the discharge/charge cycles are clearly indicated at 2.4 V for the reduction of elemental sulfur (S_8) to highly ordered polysulfides (Li_2S_x, $x \geq 4$) and at ~2.0 V for the further reduction to low-order polysulfides (Li_2S_2 and Li_2S).[37] The nanocomposite cathode material delivered a specific capacity of ~1300 mAh/g during the initial cycle, indicating ~78% electrochemical utilization (theoretical capacity = 1675 mAh/g). The commercial sulfur/carbon mixture prepared using an identical quantity of carbon to that in the composite materials, on the other hand, delivered 850 mAh/g, indicating ~51% electrochemical utilization. The nanostructure obtained from the large effective electrochemical surface area during charging/discharging and the electrical conductivity of the composite materials, which was higher than that of the commercial sulfur/carbon physical mixture, might account for the higher electrochemical utilization of the composite materials.

In addition, the electrochemical performances of the nanocomposite and the physical mixture were measured for 30 cycles at 0.1 C for a Li/S battery, as shown in Figure 5b. The initial discharge capacity was measured at ~1300 mAh/g for the nanocomposite cathode material, and the discharge capacity decreased to 796 mAh/g after 30 cycles, corresponding to ~61% capacity retention. However, the discharge capacity of the physically mixed cathode material had decreased to 415 mAh/g after 30 cycles, corresponding to ~48% capacity retention. The nanocomposite cathode material showed higher cycling stability because of the chemical interaction between the sulfur and the oxygen functional groups on the template, which may prevent the lithium polysulfide formed during charge/discharge cycling from diffusing into the electrolyte.[23,38] The sulfur/nanoparticle/RGO composites showed rate capabilities of 167.5, 837.5, and 1675 mA/g, corresponding to 0.1, 0.5, and 1.0 C, respectively, during the initial cycle (Figure S9, Supporting Information). The initial discharge capacities at 0.1, 0.5, and 1.0 C were 1295, 1214, and 1079 mAh/g, respectively. Surprisingly, the initial capacities measured at 0.5 and 1.0 C were higher than those measured in previous works. We believe that the higher rate capability was due to the high electrical conductivity of the RGO template.

The better electrochemical performance of the nanocomposites is further supported by the electrochemical impedance spectroscopy (EIS) results. The Nyquist plots in Figure 5c consist of two semicircles in the high- and

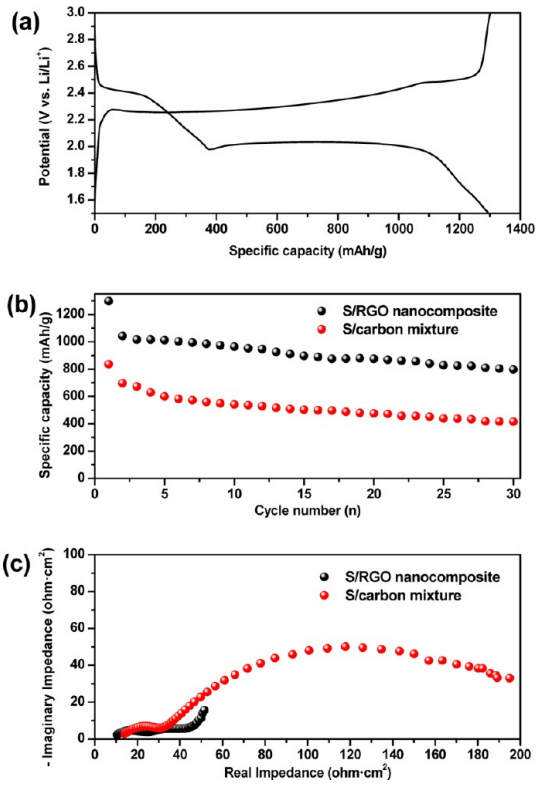

Figure 5. Electrochemical performances of sulfur nanoparticle/RGO composite: (a) initial galvanostatic charge/discharge profile measured at 0.1 C (167.5 mA/g); (b) sulfur nanoparticle/RGO composite and commercial sulfur/carbon mixture stabilities measured over 30 cycles at 0.1 C; (c) electrochemical impedance spectra for sulfur nanoparticle/RGO composite (black) and commercial sulfur/carbon mixture (red).

medium-frequency regions and a straight sloping line in the low frequency one. The high-frequency regions of both Nyquist plots show similar-sized semicircles ascribed to the formation of resistive films on the electrode surfaces in the organic electrolyte.[39,40] However, the sulfur nanoparticle/RGO composite displayed significantly less charge-transfer resistance (second semicircle in the Nyquist plot) than the physical mixture because of the enhanced electrical conductivity afforded by the chemically direct, intimate contact between the sulfur and conductive RGO sheets, which definitely improves the electrochemical performance of Li/S batteries.

CONCLUSION

We used facile, versatile solid-state methods involving nanoparticle self-assembly on carbonaceous templates to prepare Group 6A nanoparticles on the surfaces of RGO and CNTs. High-resolution TEM analysis of the prepared composites indicated that 5−10 nm sulfur nanoparticles had formed from sulfur microparticles and had uniformly dispersed on the carbonaceous surface. The oxygen functional groups on the carbonaceous material surfaces enhanced the molten sulfur or selenium wettability and acted as pinning points to form the nanoparticles. The nanoparticle size and morphology

(isolated *vs* layer-like) of the nanocomposites were regulated by tuning the oxidation state of the carbonaceous template. A considerable concentration of oxygen functional groups (<10 wt %) on the carbonaceous surface provided sites for the Group 6A nanoparticles to heterogeneously nucleate without agglomerating, so the oxygen functional groups acted like the dispersion media used in the wet-chemical method of producing isolated nanoparticles. In-depth consideration of the molten Group 6A species surface tension is also important for determining whether they will form nanocomposites with carbonaceous materials. Low surface tension molten Group 6A species could effectively wet the carbonaceous surface and were selectively located at the oxygen functional groups, forming nanoparticles anchored on the carbonaceous materials. The nanocomposite cathode materials prepared using this method for application to Li/S batteries displayed better electrochemical performance, including a higher initial capacity of 1300 mAh/g and better cycling stability, than the commercial sulfur/carbon physical mixture because of the direct chemical interaction between the sulfur nanoparticles and the RGO sheets and because the cathode nanocomposite active materials provided a larger effective electrochemical surface area and the conductive RGO sheets provided enhanced electrical conductivity.

EXPERIMENTAL METHOD

Preparation of Reduced Graphene Oxide by Solid-State Microwave Irradiation. We previously used solid-state microwave irradiation in an Ar atmosphere to prepare reduced graphene oxide (RGO) from graphite oxide.[25] The graphite oxide was prepared using Hummers method to oxidize nominally 45-μm pristine graphite flakes with concentrated sulfuric acid (H_2SO_4, 95%, Samchun Chemical Co., Ltd.), potassium permanganate ($KMnO_4$, 99%, Sigma-Aldrich), and hydrogen peroxide (H_2O_2, 35%, Junsei Chemical Co., Ltd.) in an ice bath.[41] The as-prepared graphite oxide powder (90 wt %) was then mixed with the as-prepared RGO, which acted as a microwave irradiation susceptor, in a ball mill for 1 h. The resulting uniform graphite oxide/RGO mixture was placed into a quartz bottle filled with Ar gas and was covered with a lid inside a glovebox, where the quartz bottle was tightly sealed with Paraffin tape. The quartz bottle was then placed into a microwave oven (Mars 5, CEM), and the prepared graphite oxide/RGO mixture was twice irradiated with 20 s on-time and 5 s off-time 1600 W microwave pulses, for a total of 50 s.

Preparation of Post-Treated RGO Showing Various Oxidation States. We prepared RGO sheets showing three oxidation states to prepare sulfur/RGO composites in order to systemically investigate the effects of the oxygen functional groups on the RGO sheets. As-prepared RGO showed a medium oxidation state. High-oxidation-state RGO (a-RGO), which showed a high concentration of oxygen functional groups, was prepared by vigorously stirring the as-prepared RGO with nitric acid (HNO_3, 60 wt %, Samchun Chemical Co., Ltd.), which acted as an oxidizing agent, at 70 °C for 1 h. The acid-treated a-RGO was repeatedly washed with deionized water and filtered and was subsequently freeze-dried. Low-oxidation-state RGO (HRGO900), which showed a low concentration of oxygen functional groups, was prepared by heating the as-prepared RGO at 900 °C for 4 h in an Ar atmosphere.

Preparation of Sulfur/a-RGO, Sulfur/RGO, and Sulfur/HRGO900 Composites. We ball-milled 0.5 g of the as-prepared RGO powder and either 1.0 or 2.0 g of commercial elemental sulfur (Sigma Aldrich) for 30 min to produce uniform 2:1 and 4:1 mixtures in order to prepare the sulfur/RGO composite. The mixtures were heated at 160 °C for 4 h in an Ar atmosphere in an alumina tray to obtain the sulfur/RGO composite. The sulfur/a-RGO and sulfur/HRGO900 composites were identically synthesized using 2:1 weight ratios (commercial sulfur:a-RGO or commercial sulfur:HRGO900).

Preparation of Sulfur/Pristine CNT and Acid-Treated CNT (a-CNT) Composites. We prepared CNTs showing two oxidation states as substrates for the sulfur/CNT composite: pristine CNTs (CM 95, Hanwha Nanotech), whose surfaces almost never show oxygen functional groups, and a-CNTs, pristine CNTS vigorously stirred with nitric acid (HNO_3), an oxidizing agent used to add oxygen functional groups to CNT surfaces, at 70 °C for 4 h. The a-CNTs were repeatedly washed with deionized water and filtered and were subsequently freeze-dried.

The sulfur/CNT or sulfur/a-CNT composites were synthesized using 2:1 ratios of either commercial sulfur:CNTs or commercial sulfur:a-CNTs and routes identical to that used to synthesize the sulfur/RGO composite.

Preparation of Selenium and Tellurium/RGO Composites. Either elemental Se (Sigma Aldrich) or Te (Sigma Aldrich) was mixed with the as-prepared RGO powder in a 4:1 (element:RGO) ratio. The mixtures were was ball-milled for 30 min to produce a uniform mixtures in order to prepare the Se or Te/RGO composites. The selenium and tellurium (melting points: 221 and 450 °C) mixtures were heated at 300 and 550 °C, respectively, in an alumina tray for 4 h in an Ar atmosphere.

Characterization Methods. X-ray diffraction (XRD, DMAX-2200, Rigaku) patterns were recorded at room temperature with Cu Kα radiation (λ = 1.54056 Å) and were scanned at 1°/min in 0.04° intervals in the range 5−80°. X-ray photoelectron spectroscopy (XPS, ESCA 2000, VG Microtech) was performed with monochromated Al Kα radiation ($h\nu$ = 1486.6 eV). Raman spectroscopy (Jobin-Yvon LabRAM HR) was performed at room temperature with conventional backscattering geometry and a liquid-N_2-cooled charge-coupled device (CCD) multichannel detector. A 514.5 nm wavelength argon-ion laser was used as the light source. The thermal properties of the sulfur nanoparticle/RGO composite were determined using a thermogravimetric analyzer (TGA, STA 409 PC) in an N_2 atmosphere. Thermogravimetric analysis was performed from room temperature to 600 °C while heating the samples at 10 °C/min. Nitrogen adsorption−desorption isotherms were measured on a Micromeritics ASAP ZOZO at 77 K, and the particle surface areas were calculated using the Brunauer−Emmett−Teller (BET) method. The microstructures were examined using scanning electron microscopy (SEM, JSM-7001F, JEOL, Ltd.), transmission electron microscopy (TEM, CM200, Philips), and high-resolution transmission electron microscopy (HRTEM, JEM-2100, JEOL, Ltd.). The elemental mappings were obtained using energy dispersive X-ray spectroscopy (EDX, X-MaxN, Oxford instruments).

A CR2032-coin cell was fabricated by sandwiching a porous polypropylene separator (Celgard 2400) with a lithium metal foil anode in an Ar-filled glovebox and was subsequently used to characterize the room-temperature electrochemical properties of the nanocomposite cathode materials used in the Li/S battery. The cathode electrode active material consisted of a mixture of 70 wt % sulfur nanoparticle/RGO composite, 20 wt % carbon black conducting agent, and 10 wt % polyvinylidene fluoride (PVDF) binder dissolved in *N*-methyl-2-pyrrolidone (NMP) to form slurry. A 20 μm thick doctor blade was used to uniformly coat the slurry onto an aluminum (Al) foil current collector, which was then dried at 100 °C for 24 h and was subsequently roll-pressed to 12 μm thick. Each working electrode was loaded with 2−3 mg of the cathode active materials on an Al current collector. An organic electrolyte was prepared by dissolving 1 M $LiCF_3SO_3$ and 0.2 M $LiNO_3$ in a mixture of tetra(ethylene glycol) dimethyl ether (TEGDME) and 1,3-dioxolane

(DOL) mixed in a 1:1 volumetric ratio. A galvanostatic charge/discharge test was performed using a potentiostat/galvanostat (VMP3, Biologic) in the range 1.5−3.0 V at 0.1 C (167.5 mA/g). In addition, electrochemical impedance spectroscopy (EIS) measurements were performed using the CR2032-coin cell and the same potentiostat/galvanostat at AC frequencies in the range 200 kHz to 10 mHz and at a 5 mV AC amplitude. Nyquist plots were generated specific to the area of active materials in each cathode to accurately characterize the electrical impedance of the cells. We fabricated a control cathode from a commercial sulfur/carbon black mixture containing the same amount of carbon black conducting agent as the nanocomposite and investigated its electrochemical performance in comparison with that of the nanocomposite cathode.

Conflict of Interest: The authors declare no competing financial interest.

Acknowledgment. This work was supported by the energy efficiency and resources grant (No: 20122010100140) of the Korea Institute of Energy Technology Evaluation and Planning (KETEP) funded by the Ministry of Knowledge Economy, Korean government.

Supporting Information Available: XRD patterns and SEM images of as-prepared RGO and commercial sulfur particles; N_2 adsorption isotherms for as-prepared RGO; thermogravimetric analysis of sulfur nanoparticle/RGO composite; full-scale XPS spectra for as-prepared RGO, acid-treated RGO, pristine CNTs, and acid-treated CNTs; SEM and TEM images, EDX elemental spectrum and mapping, and full-scale XPS spectrum for sulfur/CRGO composite. This material is available free of charge *via* the Internet at http://pubs.acs.org.

REFERENCES AND NOTES

1. Goesmann, H.; Feldmann, C. Nanoparticulate Functional Materials. *Angew. Chem., Int. Ed.* **2010**, *49*, 1362–1395.
2. Simon, P.; Gogotsi, Y. Materials for Electrochemical Capacitors. *Nat. Mater.* **2008**, *7*, 845–854.
3. Wang, H.; Robinson, J. T.; Diankov, G.; Dai, H. Nanocrystal Growth on Graphene with Various Degrees of Oxidation. *J. Am. Chem. Soc.* **2010**, *132*, 3270–3271.
4. Ding, Y.; Jiang, Y.; Xu, F.; Yin, J.; Ren, H.; Zhuo, Q.; Long, Z.; Zhang, P. Preparation of Nano-Structured $LiFePO_4$/Graphene Composites by Co-Precipitation Method. *Electrochem. Commun.* **2010**, *12*, 10–13.
5. Wang, D.; Kou, R.; Choi, D.; Yang, Z.; Nie, Z.; Li, J.; Saraf, L. V.; Hu, D.; Zhang, J.; Graff, G. L.; *et al.* Ternary Self-Assembly of Ordered Metal Oxide−Graphene Nanocomposites for Electrochemical Energy Storage. *ACS Nano* **2010**, *4*, 1587–1595.
6. Kim, H. K.; Bak, S. M.; Kim, K. B. $Li_4Ti_5O_{12}$/Reduced Graphite Oxide Nano-Hybrid Material for High Rate Lithium-Ion Batteries. *Electrochem. Commun.* **2010**, *12*, 1768–1771.
7. Zhu, X.; Zhu, Y.; Murali, S.; Stoller, M. D.; Ruoff, R. S. Nanostructured Reduced Graphene Oxide/Fe_2O_3 Composite as a High-Performance Anode Material for Lithium Ion Batteries. *ACS Nano* **2011**, *5*, 3333–3338.
8. Chaudhuri, R. G.; Paria, S. Synthesis of Sulfur Nanoparticles in Aqueous Surfactant Solutions. *J. Colloid Interface Sci.* **2010**, *343*, 439–446.
9. Zheng, W.; Liu, Y. W.; Hu, X. G.; Zhang, C. F. Novel Nanosized Adsorbing Sulfur Composite Cathode Materials for The Advanced Secondary Lithium Batteries. *Electrochim. Acta* **2006**, *51*, 1330–1335.
10. Yu, X.; Xie, J.; Yang, J.; Wang, K. All Solid-State Rechargeable Lithium Cells Based on Nano-Sulfur Composite Cathodes. *J. Power Sources* **2004**, *132*, 181–186.
11. Santiago, P.; Carvajal, E.; Mendoza, D.; Rendon, L. Synthesis and Structural Characterization of Sulfur Nanowires. *Microsc. Microanal.* **2006**, *12*, 690–691.
12. Gates, B.; Mayers, B.; Cattle, B.; Xia, Y. Synthesis and Characterization of Uniform Nanowires of Trigonal Selenium. *Adv. Funct. Mater.* **2002**, *12*, 219–227.
13. Sarin, L.; Sanchez, V. C.; Yan, A.; Kane, A. B.; Hurt, R. H. Selenium-Carbon Bifunctional Nanoparticles for The Treatment of Malignant Mesothelioma. *Adv. Mater.* **2010**, *22*, 5207–5211.
14. Luo, C.; Xu, Y.; Zhu, Y.; Liu, Y.; Zheng, S.; Liu, Y.; Langrock, A.; Wang, C. Selenium@Mesoporous Carbon Composite with Superior Lithium and Sodium Storage Capacity. *ACS Nano* **2013**, *7*, 8003–8010.
15. Yu, J. C.; Hu, X.; Li, Q.; Zheng, Z.; Xu, Y. Synthesis and Characterization of Core-Shell Selenium/Carbon Colloids and Hollow Carbon Capsules. *Chem.—Eur. J.* **2006**, *12*, 548–552.
16. Evers, S.; Nazar, L. F. Graphene-Enveloped Sulfur in a One Pot Reaction: A Cathode with Good Coulombic Efficiency and High Practical Sulfur Content. *Chem. Commun.* **2012**, *48*, 1233–1235.
17. Park, M. S.; Yu, J. S.; Kim, K. J.; Jeong, G.; Kim, J. H.; Jo, Y. N.; Hwang, U.; Kang, S.; Woo, T.; Kim, Y. J. One-Step Synthesis of a Sulfur-Impregnated Graphene Cathode for Lithium-Sulfur Batteries. *Phys. Chem. Chem. Phys.* **2012**, *14*, 6796–6804.
18. Wang, H.; Yang, Y.; Liang, Y.; Robinson, J. T.; Li, Y.; Jackson, A.; Cui, Y.; Dai, H. Graphene-Wrapped Sulfur Particles as a Rechargeable Lithium−Sulfur Battery Cathode Material with High Capacity and Cycling Stability. *Nano Lett.* **2011**, *11*, 2644–2647.
19. Nath, S.; Ghosh, S. K.; Panigahi, S.; Thundat, T.; Pal, T. Synthesis of Selenium Nanoparticle and Its Photocatalytic Application for Decolorization of Methylene Blue under UV Irradiation. *Langmuir* **2004**, *20*, 7880–7883.
20. Zhao, M. Q.; Liu, X. F.; Zhang, Q.; Tian, G. L.; Huang, J. Q.; Zhu, W.; Wei, F. Graphene/Single-Walled Carbon Nanotube Hybrids: One-Step Catalytic Growth and Applications for High-Rate Li−S Batteries. *ACS Nano* **2012**, *6*, 10759–10769.
21. Wang, J. Z.; Lu, L.; Choucair, M.; Stride, J. A.; Xu, X.; Liu, H. K. Sulfur-Graphene Composite for Rechargeable Lithium Batteries. *J. Power Sources* **2011**, *196*, 7030–7034.
22. Dorfler, S.; Hagen, M.; Althues, H.; Tubke, J.; Kaskel, S.; Hoffmann, M. J. High Capacity Vertical Aligned Carbon Nanotube/Sulfur Composite Cathodes for Lithium-Sulfur Batteries. *Chem. Commun.* **2012**, *48*, 4097–4099.
23. Ji, L.; Rao, M.; Zheng, H.; Zhang, L.; Li, Y.; Duan, W.; Guo, J.; Cairns, E. J.; Zhang, Y. Graphene Oxide as a Sulfur Immobilizer in High Performance Lithium/Sulfur Cells. *J. Am. Chem. Soc.* **2011**, *133*, 18522–18525.
24. Li, Z.; Wang, Y.; Kozbial, A.; Shenoy, G.; Zhou, F.; McGinley, R.; Ireland, P.; Morganstein, B.; Kunkel, A.; Surwade, S. P.; *et al.* Effect of Airborne Contaminants on The Wettability of Supported Graphene and Graphite. *Nat. Mater.* **2013**, *12*, 925–931.
25. Park, S. H.; Bak, S. M.; Kim, K. H.; Jegal, J. P.; Lee, S. I.; Lee, J.; Kim, K. B. Solid-State Microwave Irradiation Synthesis of High Quality Graphene Nanosheets under Hydrogen Containing Atmosphere. *J. Mater. Chem.* **2011**, *21*, 680–686.
26. Zhou, A.; Ma, X.; Song, C. Effects of Oxidative Modification of Carbon Surface on the Adsorption of Sulfur Compounds in Diesel Fuel. *Appl. Catal., B* **2009**, *87*, 190–199.
27. Kim, J. Y.; Kim, K. H.; Yoon, S. B.; Kim, H. K.; Park, S. H.; Kim, K. B. *In Situ* Chemical Synthesis of Ruthenium Oxide/Reduced Graphene Oxide Nanocomposites for Electrochemical Capacitor Applications. *Nanoscale* **2013**, *5*, 6804–6811.
28. Wiewiorowski, T. K.; Touro, F. J. Molten Sulfur Chemistry.1 I. Chemical Equilibria in Pure Liquid Sulfur. *J. Phys. Chem.* **1966**, *70*, 3528–3531.
29. Dujardin, E.; Ebbesen, T. W.; Hiura, H.; Tanigaki, K. Capillarity and Wetting of Carbon Nanotubes. *Science* **1994**, *265*, 1850–1852.
30. Aggarwal, R. L.; Farrar, L. W.; Polla, D. L. Measurement of the Absolute Raman Scattering Cross Sections of Sulfur and the Standoff Raman Detection of a 6-mm-thick Sulfur Specimen at 1500 m. *J. Raman Spectrosc.* **2011**, *42*, 461–464.
31. Tuinstra, F.; Koenig, J. L. Raman Spectrum of Graphite. *J. Chem. Phys.* **1970**, *53*, 1126–1130.
32. Stankovich, S.; Dikin, D. A.; Piner, R. D.; Kohlhaas, K. A.; Kleinhammes, A.; Jia, Y.; Wu, Y.; Nguyen, S. T.; Ruoff, R. S. Synthesis of Graphene-Based Nanosheets *via* Chemical Reduction of Exfoliated Graphite Oxide. *Carbon* **2007**, *45*, 1558–1565.

33. Lv, W.; Tang, D. M.; He, Y. B.; You, C. H.; Shi, Z. Q.; Chen, X. C.; Chen, C. M.; Hou, P. X.; Liu, C.; Yang, Q. H. Low-Temperature Exfoliated Graphenes: Vacuum-Promoted Exfoliation and Electrochemical Energy Storage. *ACS Nano* **2009**, *3*, 3730–3736.
34. Rozada, R.; Paredes, J.; Villar-Rodil, S.; Martínez-Alonso, A.; Tascón, J. D. Towards Full Repair of Defects in Reduced Graphene Oxide Films by Two-Step Graphitization. *Nano Res.* **2013**, *6*, 216–233.
35. Lindberg, B. J.; Hamrin, K.; Johansson, G.; Gelius, U.; Fahlman, A.; Nordling, C.; Siegbahn, K. Molecular Spectroscopy by Means of ESCA II. Sulfur Compounds. Correlation of Electron Binding Energy with Structure. *Phys. Scr.* **1970**, *1*, 286.
36. Dujardin, E.; Ebbesen, T. W.; Krishnan, A.; Treacy, M. M. J. Wetting of Single Shell Carbon Nanotubes. *Adv. Mater.* **1998**, *10*, 1472–1475.
37. Ji, X.; Lee, K. T.; Nazar, L. F. A Highly Ordered Nanostructured Carbon-Sulphur Cathode for Lithium-Sulphur Batteries. *Nat. Mater.* **2009**, *8*, 500–506.
38. Zhang, L.; Ji, L.; Glans, P. A.; Zhang, Y.; Zhu, J.; Guo, J. Electronic Structure and Chemical Bonding of a Graphene Oxide-Sulfur Nanocomposite for Use in Superior Performance Lithium-Sulfur Cells. *Phys. Chem. Chem. Phys.* **2012**, *14*, 13670–13675.
39. Ahn, W.; Kim, K. B.; Jung, K. N.; Shin, K. H.; Jin, C. S. Synthesis and Electrochemical Properties of a Sulfur-Multi Walled Carbon Nanotubes Composite as a Cathode Material for Lithium Sulfur Batteries. *J. Power Sources* **2012**, *202*, 394–399.
40. Peled, E. Electrochemical Behavior of Alkali and Alkaline Earth Metals in Nonaquous Battery Systems—The Solid Electrolyte Interface Model. *J. Electrochem. Soc.* **1979**, *126*, 2047–2051.
41. Hummers, W. S.; Offeman, R. E. Preparation of Graphitic Oxide. *J. Am. Chem. Soc.* **1958**, *80*, 1339–1339.